

Model Reduction for Transport-Dominated Problems via Cross-Correlation Based Snapshot Registration

Harshith Gowrachari^{*1}, Giovanni Stabile^{†2}, and Gianluigi Rozza^{‡1}

¹Mathematics Area, mathLab, International School for Advanced Studies, via Bonomea 265, 34136 Trieste, Italy

²Biorobotics Institute, Sant'Anna School of Advanced Studies, V.le R. Piaggio 34, 56025, Pontedera, Pisa, Italy.

Abstract

Traditional linear approximation methods, such as proper orthogonal decomposition and the reduced basis method, are ill-suited for transport-dominated problems due to the slow decay of the Kolmogorov n -width, leading to inefficient and inaccurate reduced-order models. In this work, we propose a model reduction approach for transport-dominated problems by employing cross-correlation based snapshot registration to accelerate the Kolmogorov n -width decay, thereby enabling the construction of efficient and accurate reduced-order models using linear approximation methods. We propose a complete framework comprising offline-online stages for the development of reduced order models using the cross-correlation based snapshots registration. The effectiveness of the proposed approach is demonstrated using two test cases: 1D travelling waves and the higher-order methods benchmark test case, 2D isentropic convective vortex.

Keywords: non-linear model order reduction, registration method, cross-correlation, transport-dominated problems, reduced order modelling.

1 Introduction

Reduced order modelling is a rapidly advancing field in computational science and engineering. Industries have a keen interest in obtaining reduced order models (ROMs) for engineering systems, particularly in applications involving control, optimization, and uncertainty quantification. ROMs offer significant computational efficiency in many query scenarios and are suitable for real-time computations. These models achieve computational efficiency by approximating high-dimensional parametric partial differential equations (PDEs) solutions with low-dimensional representations, substantially reducing

^{*}hgowrach@sissa.it

[†]giovanni.stabile@santannapisa.it

[‡]grozza@sissa.it

the computational cost compared to full-order models (FOMs).

To obtain the FOM solutions of the parametric PDEs describing real-world scenarios, discretization methods such as the finite element method (FEM) and finite volume method (FVM) are widely employed. Although these methods ensure accuracy, they are computationally expensive. ROM framework mitigates this challenge through a two-stage approach:

- Offline (training) stage – This computationally expensive phase involves generating full-order model (FOM) solutions (snapshots) and constructing the ROM by approximating the high-dimensional solution manifold with a low-dimensional approximation subspace.
- Online (testing and predictive) stage – This significantly more efficient phase utilizes the low-dimensional approximation subspace obtained during the offline stage to rapidly predict reduced solutions for new, unseen parameters, substantially reducing computational expenses.

Several model reduction techniques are available to obtain the low-dimensional approximation subspaces [38, 18, 7, 41]. Among these, linear approximation methods such as proper orthogonal decomposition (POD) and reduced basis (RB) methods are widely used and highly effective in various applications. However, certain problems of interest, such as transport-dominated problems, exhibit slow decay of Kolmogorov n -width (KnW). This slow decay of KnW limits the model reduction achievable through linear subspace approximations [37].

The solution manifolds of the transport-dominated problems, such as travelling waves, convective vortex, and vortex shedding, exhibit slow decay of the Kolmogorov n -width (KnW), making it difficult to obtain a low-dimensional linear approximation subspace for the construction of accurate and efficient ROMs. The KnW, as defined in [37], provides a rigorous measure of the reducibility of the solution manifold \mathcal{M} using linear approximation subspaces.

For a solution manifold \mathcal{M} comprising f elements (solutions across all time instances) embedded in a normed linear space $(X_N, \|\cdot\|_{X_N})$, the Kolmogorov n -width $d_n(\mathcal{M})$ is defined as:

$$d_n(\mathcal{M}) := \inf_{E_n \subset X_N} \sup_{f \in \mathcal{M}} \inf_{g \in E_n} \|f - g\|_{X_N} \quad (1)$$

where E_n is a linear subspace of X_N with dimension n . The KnW $d_n(\mathcal{M})$ represents the maximum approximation error obtained when any element $f \in \mathcal{M}$ is approximated by an element $g \in E_n$. Furthermore, as faster the $d_n(\mathcal{M})$ decay with increasing n , indicates the effectiveness of an n dimensional low-dimensional linear subspace is in approximating the solution manifold \mathcal{M} .

Recent advancements in model-reduction techniques have focused on addressing the challenges posed by slow Kolmogorov n -width decay, being the main reason for the development of non-linear approaches [34]. These methods include performing model reduction on non-linear manifolds, such as constructing non-linear trial subspaces using convolutional autoencoders (CAEs) [23, 17, 8, 19, 26, 12, 24, 40], and employing quadratic approximation manifolds [22, 2, 13]. Other strategies involve incorporating adaptive enrichment techniques, [16, 51, 35, 33, 4], and transforming linear subspaces through transport maps using registration methods [32, 27, 20, 28, 5, 39, 47, 49, 31, 30]. These registration based approaches yield a low-dimensional transformed linear subspace that effectively approximates full-order solutions.

In this work, we employ cross-correlation based snapshot registration for model reduction of transport-dominated problems. This approach leverages cross-correlation to align multiple snapshots to a reference, accelerating the decay of KnW and yielding a low-dimensional approximation subspace for the construction of efficient ROMs. It is particularly effective in scenarios where conventional linear approximation methods struggle, providing a more robust framework for capturing the system's essential dynamics, and enabling the construction of efficient and accurate ROMs using the transformed linear approximation subspace obtained through registration.

In reduced-order modelling, once the reduced approximation subspace is obtained, it is essential to compute the evolution of the dynamics within this subspace. This requires determining the modal coefficients or latent coordinates, which can be achieved through either intrusive or non-intrusive methods. In the intrusive approach, the discretized governing equations (PDEs) are projected onto the low-dimensional subspace, resulting in a system of low-dimensional ODEs. This procedure, known as Galerkin or Petrov-Galerkin projection based ROM, is discussed in [44, 45]. In this work, we focus specifically on non-intrusive methods, where, after obtaining the set of snapshots (FOM solutions), the ROM is constructed using proper orthogonal decomposition (POD) with regression (POD-R) strategy. This method is discussed in detail in the following section.

This article is organized as follows, in section 2 we discuss the construction of a non-intrusive or data-driven reduced order model using POD with regression (POD-R) strategy; in section 3 we discuss the employment of the cross-correlations based snapshots registration approach; in section 4 the implementation of the complete algorithm for the development of ROM utilizing the cross-correlations based registration is mentioned; in section 5 we test our proposed approach by applying to transport-dominated problems, 1D travelling waves and 2D isentropic convective vortex; and in section 6 the conclusions, perspectives, and future directions are discussed.

After working on this manuscript, we came across the work [21], which closely aligns with the framework we propose. In their approach, cross-correlation based snapshot registration, a widely used technique in medical imaging [3, 6], is integrated with the

operator inference framework [36] for the construction of ROMs. This framework is referred to as shift operator inference [21], where shifts are obtained via cross-correlation. In this work, we integrate cross-correlation based snapshot registration within the non-intrusive data-driven ROM framework [48].

2 Reduced-order modelling of time-dependent problems

In this work, we are focusing on time-dependent problems, considering the abstract partial differential equation (PDE) as shown given in (2), defined over the domain $\Omega \subset \mathbb{R}^n$ and the time interval $T = [0, t_f]$:

$$\mathcal{L}(s(t)) = 0, \quad t \in T. \quad (2)$$

Where $s(t)$ is an unknown function, the operator \mathcal{L} incorporates the differential operators, forcing terms and boundary conditions that govern the dynamics of $s(t)$. To obtain the full-order solutions of the given time-dependent problem, here we consider the finite-difference method, but one can choose to use any discretization method, such as the finite-volume method or finite-element method, and later, followed by a time integration scheme. We denote the solutions database as a set of time-snapshot pairs given by $\{t_i, s_i\}_{i=1}^{N_T}$ with $t_i \in T \subset \mathbb{R}^{N_T}$ with N_T number of time instances and $s_i \in \mathbb{R}^{N_h}$ with N_h number of degrees of freedom. We represent the snapshots matrix $S \in \mathbb{R}^{N_h \times N_T}$ as :

$$S = \begin{bmatrix} | & | & & | \\ s_1 & s_2 & \dots & s_{N_T} \\ | & | & & | \end{bmatrix}. \quad (3)$$

To reduce the computational cost of the associated discretization method, in this section, we present the general framework for non-intrusive ROMs using proper orthogonal decomposition with regression (POD-R) strategy [48]. Here, we first recall the proper orthogonal decomposition, a widely used linear approximation method in the ROM community, which is exploited together with the regression strategy to obtain efficient and accurate ROMs.

2.1 Proper orthogonal decomposition

We use POD to obtain the reduced linear approximation subspace U_r , where $\dim(U_r) = N_r \ll N_h$, which consists of POD modes spanned column-wise. The POD modes are obtained by performing singular value decomposition (SVD) [46] of the snapshots matrix:

$$S = U \Sigma V^T, \quad (4)$$

where, $U \in \mathbb{R}^{N_h \times N_h}$ and $V \in \mathbb{R}^{N_T \times N_T}$ are the two orthonormal matrices. $\Sigma \in \mathbb{R}^{N_h \times N_T}$ is the diagonal matrix with r non-zero singular values, arranged in descending

order $\sigma_1 \geq \sigma_2 \geq \dots \geq \sigma_r > 0$, which indicates the energy contribution of the corresponding modes. Here, r is the rank of the snapshot matrix S . The reduced linear approximation subspace $U_r \in \mathbb{R}^{N_h \times N_r}$ is constructed such that :

$$\mathbf{U}_r = \underset{\hat{\mathbf{U}} \in \mathbb{R}^{N_h \times N_r}}{\operatorname{argmin}} \frac{1}{\sqrt{N_T}} \|\mathbf{S} - \hat{\mathbf{U}} \hat{\mathbf{U}}^T \mathbf{S}\|_F \quad (5)$$

where $\|\cdot\|_F$ is a frobenius norm and S is the snapshots matrix.

The POD modes are column entries of the left singular matrix U corresponding to the largest singular values. The energy retained by the first m modes is given by the ratio of the energy contained by the first m modes and the energy contained by all r modes :

$$E(m) = \frac{\sum_{i=1}^m \sigma_i^2}{\sum_{i=1}^r \sigma_i^2}. \quad (6)$$

Generally, the reduced space U_r is constructed by considering the first N_r columns of U [11], such that the $E(N_r)$ contains a user-defined threshold, usually about 95 – 99.9% of the cumulative energy.

2.2 POD with regression

In this work, POD with regression (POD-R) strategy is employed to obtain non-intrusive data-driven ROM [48], which exploits regression to approximate the trajectories of the full-order model. Once we have the reduced space U_r , we approximate the solutions of $s(t)$ by reduced expansion:

$$s(t) = U_r c_r(t) \quad (7)$$

where, $c_r \in \mathbb{R}^{N_r}$ is the temporal expansion coefficients. We compute the temporal expansion coefficients as shown in (8), by projecting the snapshot matrix S onto the reduced subspace U_r .

$$c(t_i) = U_r^T s(t_i) \quad \forall i = 1, \dots, N_{train}. \quad (8)$$

Following the previous steps, we can only approximate the snapshots of the initial database (training set) via these temporal expansion coefficients. To predict snapshots for new time instances, we need to build a map from time t_i to c_i temporal expansion coefficients. Here, the main aim is to construct a regression $\mathcal{I} : T \mapsto \mathbb{R}^{N_r}$ which approximates the map \mathcal{F} as in (9) given by a set of N_{train} input-output pairs $\{t_i, c_i\}_{i=1}^{N_{train}}$, where t_i is the time associated with the i^{th} snapshot and c_i are the corresponding temporal coefficients obtained by (8).

$$\mathcal{F} : t \in T \mapsto c \in \mathbb{R}^{N_r}. \quad (9)$$

To construct this regression \mathcal{I} , there are various techniques available, such as linear interpolation, Gaussian process regression (GPR), radial basis function (RBF) interpolation, multi-fidelity methods, and artificial neural networks (ANNs), to name a few. In

this work, we exploit radial basis function (RBF) interpolation to devise this map. The constructed regression model is used to predict the snapshot s^* for new time instance t^* via inverse coordinate transformation:

$$\mathbf{s}(t^*) = U_r I(t^*). \quad (10)$$

3 Cross-correlation based snapshot registration

Cross-correlation measures the similarity between two signals as a function of the displacement or lag between them. It plays a crucial role in signal processing, pattern recognition, time series analysis, and filtering. Cross-correlation aids in identifying or quantifying the relationships between signals and is used to detect signals that are embedded in noise. Image registration through cross-correlation is an essential and widely adopted technique in the field of medical imaging [3, 6]. In this work, we exploit cross-correlation to register the snapshots of transport-dominated problems and aim to accelerate the KnW decay.

Continuous Cross-Correlation: Let us consider two continuous functions $f(t), g(t) \in \mathbb{C}$. The continuous cross-correlation between f and g is defined as:

$$(f \star g)(\tau) \triangleq \int_{-\infty}^{\infty} \overline{f(t)} g(t + \tau) dt \quad (11)$$

where $\overline{f(t)}$ denotes the complex conjugate of $f(t)$, and τ is the time lag or displacement. The cross-correlation measures the similarity between $f(t)$ and a time-shifted version of $g(t)$, integrating the product of complex conjugate $\overline{f(t)}$ and the shifted $g(t + \tau)$ over all time.

Discrete Cross-Correlation: Let us consider two discrete signals $f[n], g[n] \in \mathbb{C}^{N_h}$, where N_h is the number of elements in the signals. The discrete cross-correlation between f and g is defined as:

$$(f \star g)[k] \triangleq \sum_{n=0}^{N_h-1} \overline{f[n]} g[n + k] \quad (12)$$

where $\overline{f[n]}$ is the complex conjugate of the discrete signal $f[n]$, n denotes the index of the signal elements, and k is the displacement or lag. The discrete cross-correlation is computed by summing the element-wise product between $\overline{f[n]}$ and the shifted sequence $g[n + k]$. Depending on the context, $g[n + k]$ may be assumed to be zero outside its defined range (zero-padding) or periodically extended (circular correlation).

Cross-correlation offers a robust framework for analyzing the relationship between time-shifted signals. In this work, we leverage cross-correlation snapshot registration, as outlined in Algorithm 1. In this framework, snapshots are treated as discrete signals,

and the cross-correlation between each snapshot s_i and the reference snapshot s^{ref} is used to compute the shifts required for registration. Here, we employ the registration of snapshots via cross-correlation to circumvent KnW decay for transport-dominated problems. This method aims to determine the optimal shift for each snapshot, aligning them with the reference based on the maximization of their cross-correlation.

The process of cross-correlations based registration is as follows: First, we select a set of training snapshots $\{s_1, s_2, \dots, s_{N_{\text{train}}}\}$ corresponding to time instances $\{t_1, t_2, \dots, t_{N_{\text{train}}}\}$, and choose one snapshot as the reference s^{ref} . For each training snapshot s_i , we compute the cross-correlation¹ between the reference s^{ref} and the snapshot s_i at various time shifts (lags). Cross-correlation measures the similarity between two signals as a function of their relative time shifts. The optimal shift Δ_i for each snapshot s_i is determined by identifying the shift that maximizes the cross-correlation, i.e., the shift that yields the highest similarity between the reference and the respective snapshot s_i . Once the optimal shift Δ_i is determined for each snapshot s_i , these shifts are employed to align the snapshots with the reference s^{ref} . Then, we store the registered snapshots s_i^{ref} and their corresponding optimal shifts for subsequent steps in developing the ROM.

4 ROM via cross-correlation based snapshot registration

In this section, we present the complete workflow for constructing reduced-order models (ROMs) using the cross-correlation based snapshot registration framework. As outlined in Algorithm 2, the workflow consists of two stages: (1) the offline stage, where snapshots are registered and the ROM is constructed, and (2) the online stage, the ROM predictions which are at the reference are reverted to the correct physical frame.

In the offline phase, the snapshots are registered using Algorithm 1, which exploits cross-correlation to employ registration and yields a registered snapshots matrix S^{ref} and a corresponding shifts matrix Δ . Now, all the snapshots are in the reference frame, accelerating the KnW and yielding a low-dimensional linear approximation subspace. We construct ROM² utilizing the registered snapshots matrix S^{ref} , following the steps mentioned in section 2, with radial basis function (RBF) interpolation used for regression. To obtain shifts for new time instances in the online phase, we construct a map α using a regression on the training pairs $\{t_i, \Delta_i\}$. In the online phase, the ROM predictions are initially at the reference frame, and we exploit the corresponding optimal shift obtained by the map α to revert the snapshots to the correct physical frame.

¹We use `scipy` python library to compute correlation

²using EZyRB package [10], a Python library for data-driven ROMs.

Algorithm 1 : Registration via cross-correlation

- 1: **Input:** Set of training snapshots $\{s_1, s_2, \dots, s_{N_{train}}\}$ for corresponding time instances $\{t_1, t_2, \dots, t_{N_{train}}\}$, reference snapshot s^{ref}
- 2: **Output:** Set of Registered snapshots $\{s_1^{\text{ref}}, s_2^{\text{ref}}, \dots, s_{N_{train}}^{\text{ref}}\}$, corresponding shifts $\Delta = \{\Delta_1, \Delta_2, \dots, \Delta_{N_{train}}\}$
- 3: **for** each snapshot s_i in set of training snapshots **do**
- 4: Compute discrete cross-correlation between the reference snapshot s^{ref} and the snapshot s_i :
$$\text{correlation}(s^{\text{ref}}, s_i) = \text{correlate}(s^{\text{ref}}, s_i)$$
- 5: Obtain optimal shift Δ_i :
$$\Delta_i = \text{argmax} \left(\text{correlation}(s^{\text{ref}}, s_i) \right) - (N_h - 1)$$
- 6: To register snapshots: Apply the shift Δ_i to the snapshot s_i using circular shift:
$$s_i^{\text{ref}} = \text{shift}(s_i, \Delta_i)$$
- 7: Store the Registered snapshot s_i^{ref} and the shift Δ_i
- 8: **end for**
- 9: **return** the set of Registered snapshots $S^{\text{ref}} = \{s_1^{\text{ref}}, s_2^{\text{ref}}, \dots, s_{N_{train}}^{\text{ref}}\}$ and shifts Δ_i .

Algorithm 2 : ROM via cross-correlation based snapshot registration

- 1: **Input:** Set of training snapshots $\{s_1, s_2, \dots, s_{N_{train}}\}$ for corresponding time instances $\{t_1, t_2, \dots, t_{N_{train}}\}$, reference snapshot s^{ref} , N_r number of POD modes.
- 2: **Output:** Prediction of snapshots via cross-correlation based snapshots registration.
Offline stage
- 3: Registration of snapshots via cross-correlation using Algorithm 1:
Obtain the Registered snapshots matrix S^{ref} and the corresponding optimal shifts matrix Δ
- 4: Construct ROM on the registered snapshots matrix S^{ref} following the steps in section 2.

$$\text{rom} = \text{ROM}(S^{\text{ref}}, \text{POD}, \text{RBF})$$

- 5: Construct map α using regression for $\{t_i, \Delta_i\}$ pairs: To predict shifts for new time instances in the online phase.

Online stage

- 6: **for** each new time instance t_i in test set: **do**
- 7: $s_i^{\text{ref}} = \text{rom.predict}(t_i)$
- 8: Obtain the optimal shift Δ_i^* using map α .
- 9: Transport back the predicted snapshots to the correct physical frame by reverting them with the optimal shift:

$$s_i = \text{shift}(s_i^{\text{ref}}, -\Delta_i^*)$$

- 10: **end for**
- 11: **return** the set of predicted snapshots $\{s_1, s_2, \dots, s_{N_{test}}\}$ in correct physical frame.

5 Numerical experiments

In this section, we evaluate the proposed approach to model reduction using cross-correlation based snapshot registration to construct ROMs for transport-dominated problems. We consider two numerical experiments: the 1D travelling waves and a higher-order benchmark test case - the 2D isentropic convective vortex.

5.1 1D Travelling wave

We consider a parameterized 1D Gaussian function (13) to mimic the solutions of the linear transport equation considered in [12, 13, 15], with $\beta = 1$, $x \in [0, 10.25]$ is the spatial coordinate, constant σ (standard deviation), and $t \in [0, 10.25]$ is the mean, interpreted here as time to treat this as a parameterized time-dependent problem. We generate a database consisting of 100 time instances and their corresponding snapshots over the 256 equidistant spatial nodes in $x \in [0, 10.25]$. We divide 50% of the database as a training set and the rest as a testing set, as shown in the Figure (1)

$$f(t) = \beta e^{-(x-t)^2/(2\sigma^2)}. \quad (13)$$

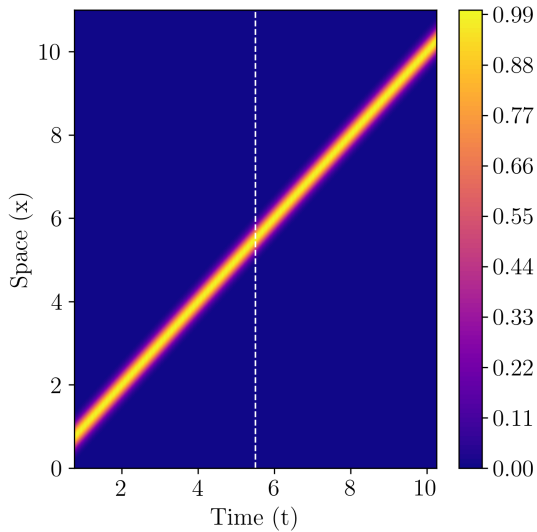


Figure 1: 2D contour of the original snapshots of the 1D travelling waves. Here, the white line separates the first 50% dataset as the training set and the rest as the test set.

In the offline phase, we select the reference snapshot corresponding to the parameter $t = 3.03$. Using the procedure outlined in Algorithm 1, we perform snapshot registration, aligning multiple snapshots to the reference by leveraging cross-correlation based registration, as shown in Figure 2. From Figure 3 it is evident that the registration

significantly accelerates the KnW decay, leading us to seek a low-dimensional linear approximation subspace for efficient ROM construction. Figure 3b presents the first POD mode obtained by employing registration, which captures the structure of the Gaussian travelling waves, alongside the first 10 POD modes of the unregistered snapshots. In the case of unregistered snapshots, we have to consider numerous POD modes to construct ROM, which leads to inefficient ROMs. We construct ROM by considering the first POD mode (with 99.99 % of cumulative energy) obtained via registration, and we exploit the POD-R strategy discussed in section 2. Here, we utilize the radial basis function (RBF) interpolation for the regression task.

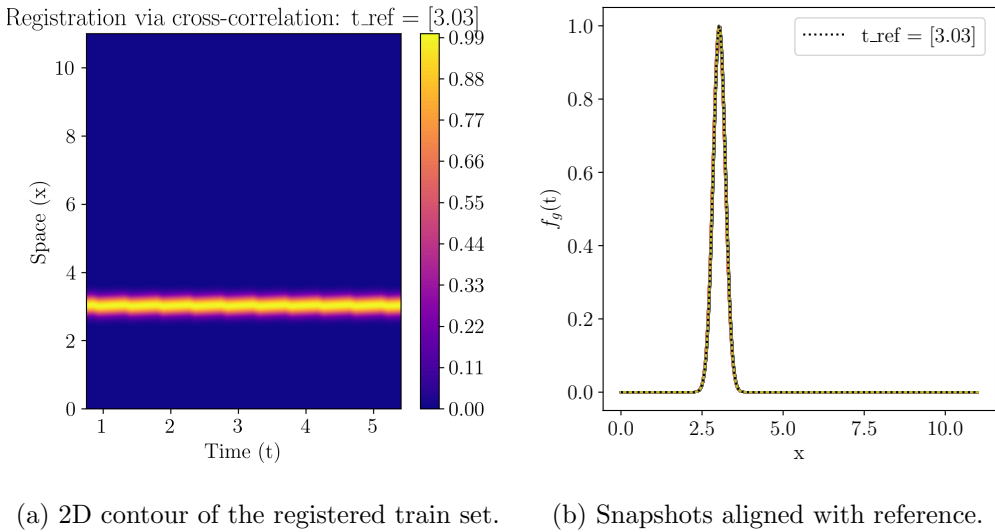
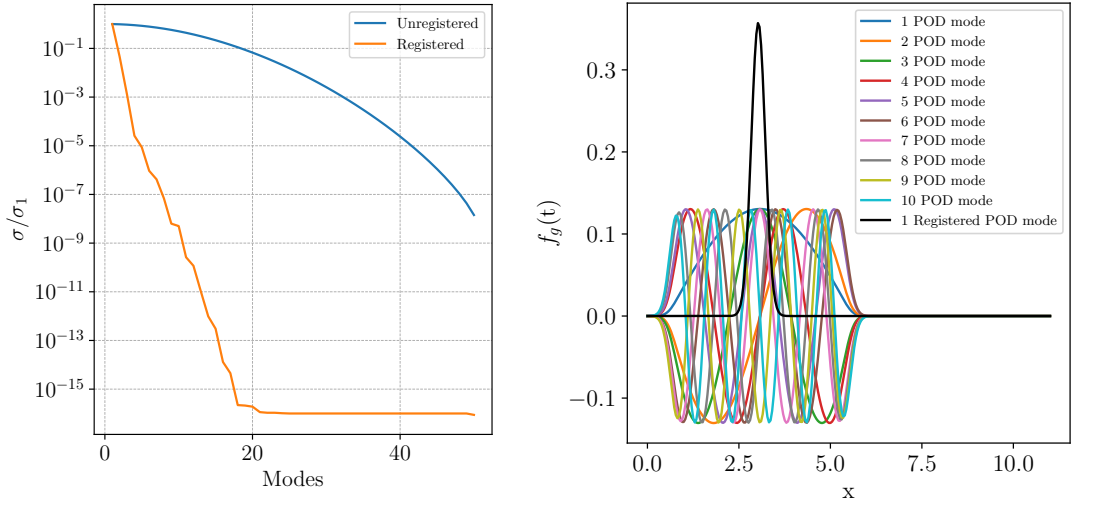


Figure 2: 1D travelling waves training set registered at the reference configuration.

After constructing the ROM, we incorporate shifts in the online phase by mapping parameter t_i to the optimal shift Δ_i (denoted as α in Algorithm 2) using linear interpolation. To predict snapshots at new time instances, we employ the regression α to transform the ROM-predicted snapshots (in the reference frame) back to the correct physical frame. Figure 4 presents the predicted snapshots in the correct physical frame for both train and test set parameters, alongside the original snapshots (ground truth) and the absolute differences between predictions and ground truth. The relative prediction error, shown in Figure 5, reveals that test errors are an order of magnitude larger than training errors, with the mean relative error highlighted.

In Figure 6, we present the mean relative L_2 prediction error for test set parameters, with varying POD ranks, for the construction of POD-RBF-ROM, both unregistered and registered snapshots via cross-correlation. It is evident that in the unregistered case, even after considering 25 modes (with 99.99 % cumulative energy), it leads to inefficient and inaccurate ROMs even for simple linear transport problems, with errors



(a) Singular values decay comparison

(b) 1D travelling wave registered POD mode

Figure 3: **Left:** Comparison of the singular values of registered and unregistered 1D travelling waves. **Right:** The first 10 POD modes obtained from the unregistered snapshots, alongside the 1st POD mode obtained via cross-correlation based snapshot registration.

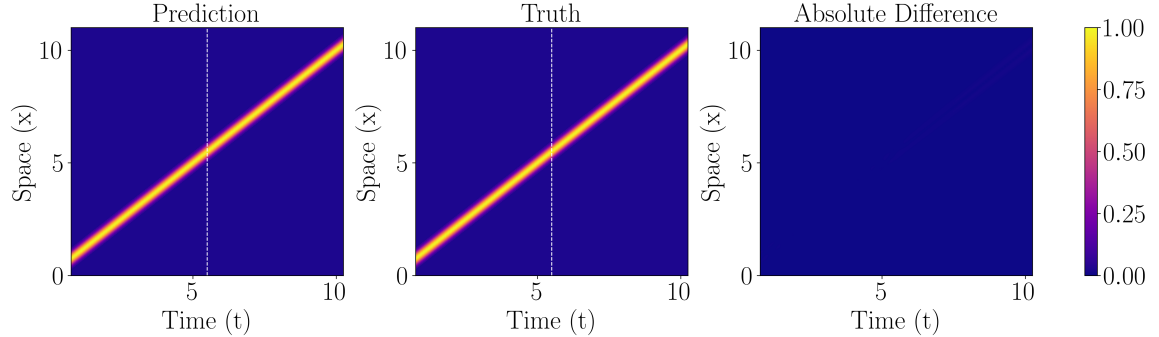


Figure 4: Comparison of the predictions of the resulting ROM of the 1D travelling waves with the original snapshots as ground truth, here the white line separates the first 50% dataset as the training set and the remaining as the test set and also shows the absolute difference between the prediction and the ground truth.

two orders of magnitude larger than in the registered case. In contrast, for the registered case, the first mode (retaining 99.99% of the cumulative energy) results in an efficient and accurate ROM.

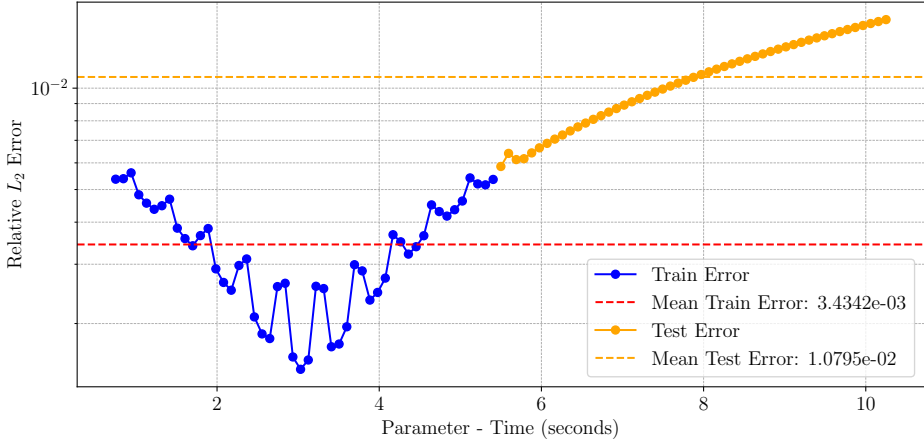


Figure 5: Relative L_2 predictions error by the ROM of the 1D travelling wave via cross-correlation based snapshots registration, for both training set and test set parameters.

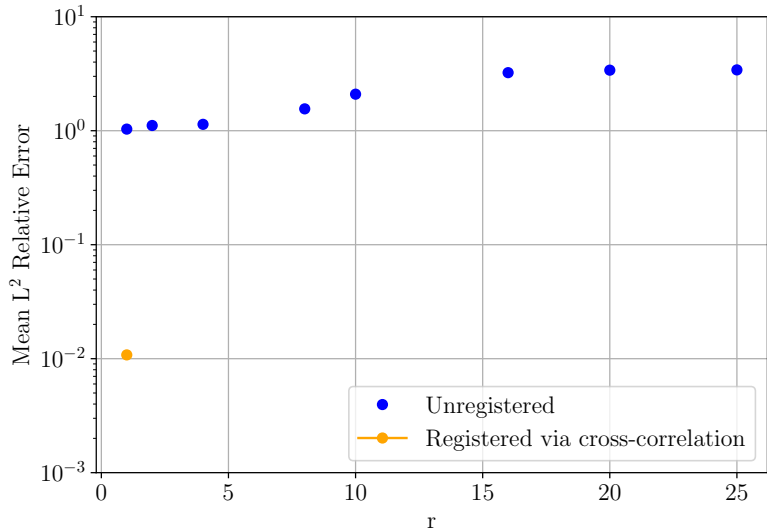


Figure 6: Comparison of mean relative L_2 prediction error for 1D travelling wave test set parameters using POD-RBF-ROM, presented for the unregistered case (without registration) and the registered case (with registration via cross-correlation).

5.2 2D isentropic convective vortex

For the second experiment, we consider the 2D isentropic convective vortex, a popular higher-order method benchmark case [43, 50]. To describe the flow physics of the inviscid, compressible flow of our benchmark case, we consider the 2D Unsteady Euler equations:

$$\frac{\partial}{\partial t} \begin{bmatrix} \rho \\ \rho u \\ \rho v \\ E \end{bmatrix} + \frac{\partial}{\partial x} \begin{bmatrix} \rho u \\ \rho u^2 + p \\ \rho u v \\ u(E + p) \end{bmatrix} + \frac{\partial}{\partial y} \begin{bmatrix} \rho v \\ \rho u v \\ \rho v^2 + p \\ v(E + p) \end{bmatrix} = 0 \quad (14)$$

where, ρ is density, (u, v) are velocity x and y component, p is pressure and E is total energy. In this test case, we consider constant specific heat ratio, $\gamma = 1.4$, and gas constant, $R_{gas} = 287.15 \text{ J/Kg.K}$. The thermodynamic closure is attained by the total energy equation (15).

$$E = \frac{p}{\gamma - 1} + \frac{1}{2} \rho (u^2 + v^2). \quad (15)$$

$$\begin{cases} \rho = \left[1 - \frac{(\gamma-1)b^2}{8\gamma\pi^2} e^{1-r^2} \right]^{\frac{1}{\gamma-1}}, \\ p = \rho^\gamma, \\ u = u_\infty - \frac{b}{2\pi} e^{\frac{1}{2}(1-r^2)} (y - y_c), \\ v = v_\infty + \frac{b}{2\pi} e^{\frac{1}{2}(1-r^2)} (x - x_c). \end{cases} \quad (16)$$

The freestream flow is initialized with the conditions $\rho_\infty = 1$, $u_\infty = 0.1$, $v_\infty = 0$, and $p_\infty = 1$. The vortex is introduced into the domain based on the analytical solution described in (16), with a vortex strength of $b = 0.5$, a vortex radius $r = \sqrt{(x - x_c)^2 + (y - y_c)^2} = 0.5$, and a vortex centre located at $(x_c, y_c) = (5, 10)$. There are several vortex problems reported in the literature [42]. In this study, we adopt the version implemented in the HyPar 1.0 package — finite difference hyperbolic-parabolic PDE solver on cartesian grids [9] and we use this package to obtain the full-order solution of the equation 14.

To approximate the spatial derivatives in the governing equations, we employ the fifth-order hybrid-compact weighted essentially non-oscillatory (WENO) scheme, a high-order accurate numerical method designed for hyperbolic partial differential equations and convection-dominated problems [52]. For time integration, we consider the third-order strong stability-preserving Runge-Kutta (SSPRK3) method [14].

We consider the rectangular computational domain $\Omega = [0, 40] \times [0, 20]$, discretized into 28,800 cartesian grid points. To introduce a vortex into the domain, we use the initial conditions given in (16). The simulation is performed over the time interval $t \in [0, 62.5]$ using a time step of $\Delta t = 0.00625$. Snapshots are recorded every 100 time-steps Δt , resulting in a snapshot matrix containing density field snapshots at $N_T = 100$ time instances. The full-order solutions (snapshots) at three different time instances are shown in Figure 7.

In this numerical experiment, we consider the first 30% dataset as a training set and the remaining 70% as the test set. We perform registration on the training set, Figure

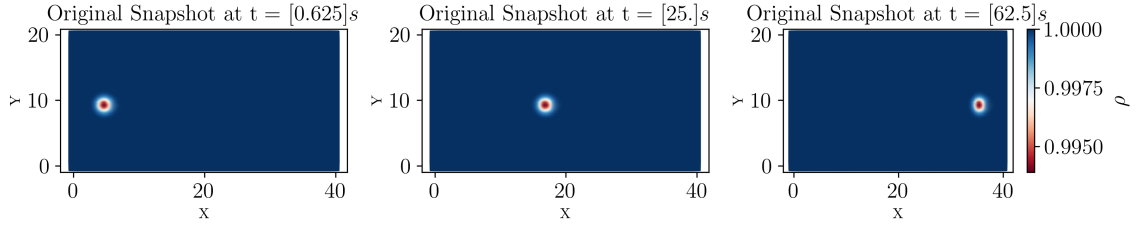


Figure 7: Full-order solutions of the isentropic convective vortex at time instances, $t \in \{0.625, 25, 62.5\}$.

8 presents the registered snapshots at time instances $t \in \{0.625, 25, 62.5\}$, comparing with the reference and the corresponding original snapshot. We perform reduction using POD on both the registered snapshots matrix and unregistered snapshots matrix, the singular values decay is shown in Figure 9a with sharp decay for registered snapshots. Furthermore, Figure 9b illustrates the POD modes obtained from the registered snapshots, which accurately capture the vortex structure (first row of Figure 9b). In contrast, the POD modes from the unregistered snapshots fail to capture the vortex structure effectively (second row of Figure 9b).

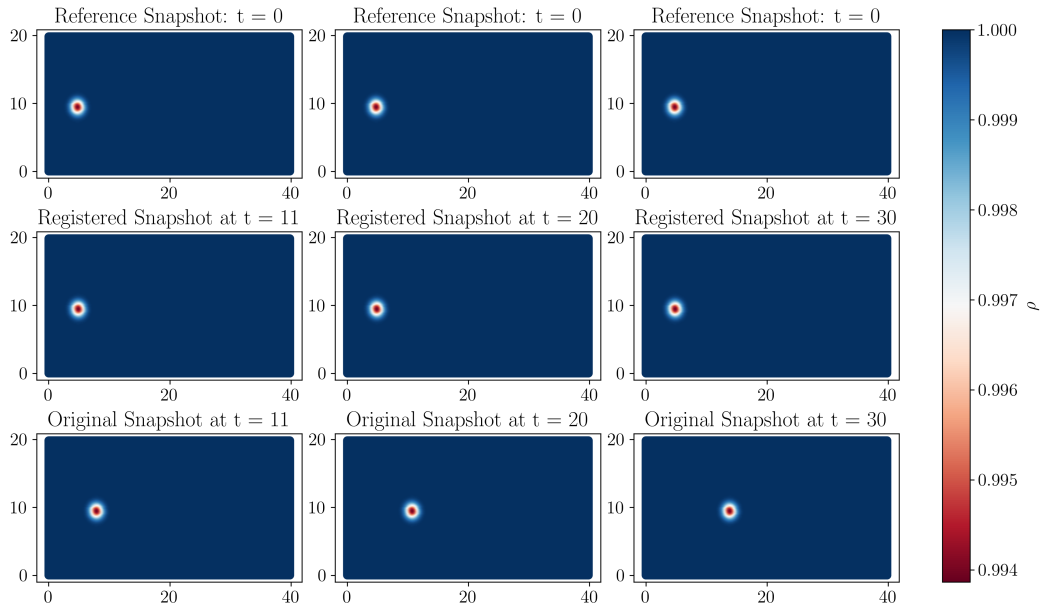


Figure 8: Comparison of the isentropic convective vortex registered snapshots with the reference and the corresponding original snapshot.

We utilize the first POD mode obtained via registration and as previously, we employ the POD-R strategy to construct ROM for this numerical experiment. To employ shifts

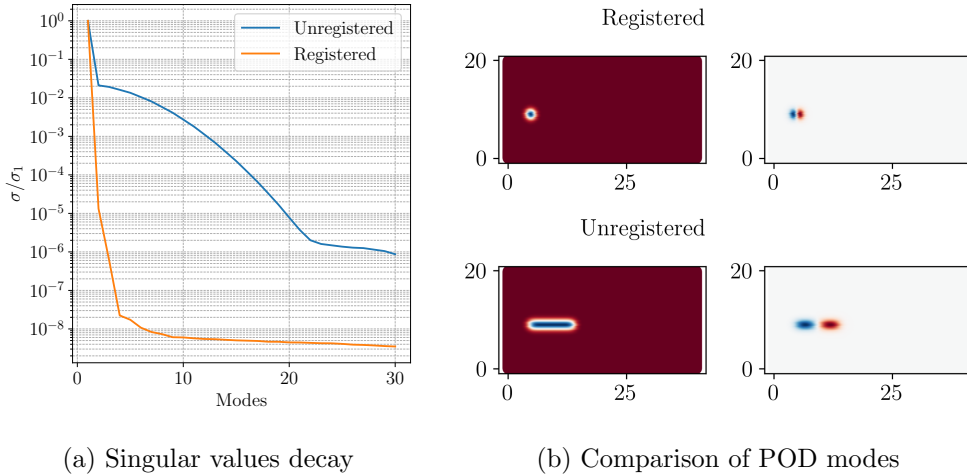


Figure 9: **Left:** Comparison of singular values decay of registered snapshots matrix, labelled as Registered and of the unregistered snapshots matrix as Unregistered. **Right:** Showing the first two modes of the registered snapshots (first row - Registered) and showing the first two modes of the unregistered snapshots matrix (second row - Unregistered).

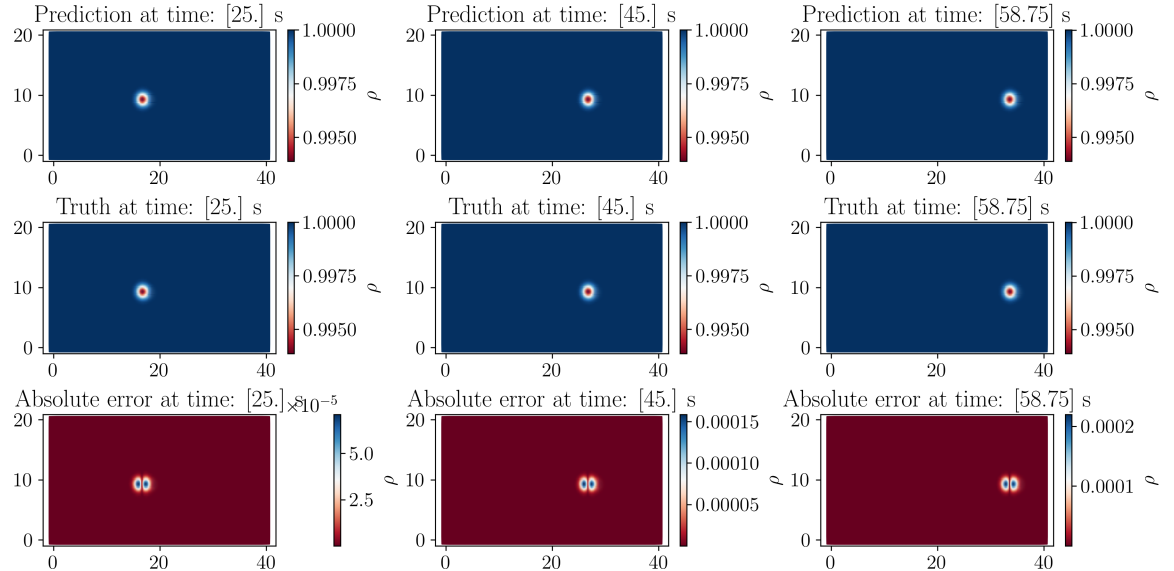


Figure 10: Predicted snapshots using POD-RBF-ROM with cross-correlation based registration for the isentropic convective vortex test set parameters at time instances $t \in \{25, 45, 58.75\}$ s.

in the online phase, we again use linear interpolations to build parameter t_i to optimal shift Δ_i mappings. As specified in the previous case in the online phase, we utilize the

predicted optimal shifts alongside the ROM prediction to revert the predicted snapshots to the correct physical frame. The predicted snapshots in the correct physical frame for three-time instances $t \in \{25, 45, 58.75\}$ from the test set are shown in Figure 10, with the corresponding original snapshot as ground truth and the absolute difference. The prediction error for both the training and test set parameters is presented in 11. The relative L_2 error of the predicted snapshots is plotted for each parameter, along with the mean relative L_2 error.

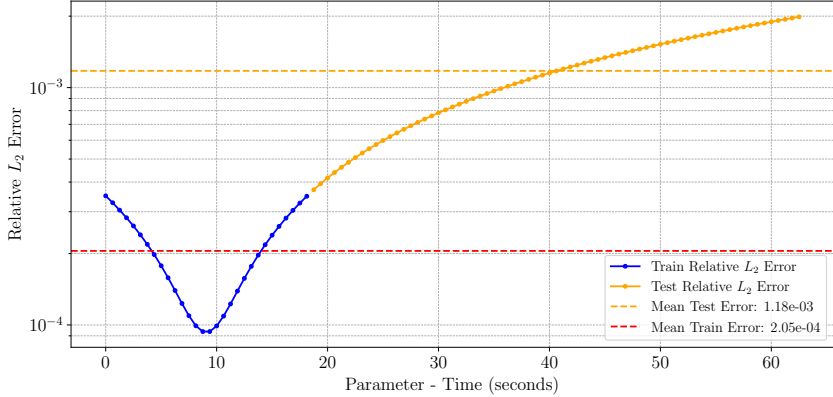


Figure 11: Relative L_2 predictions error of the isentropic convective vortex ROM via cross-correlation based registrations, for both training and test set parameters.

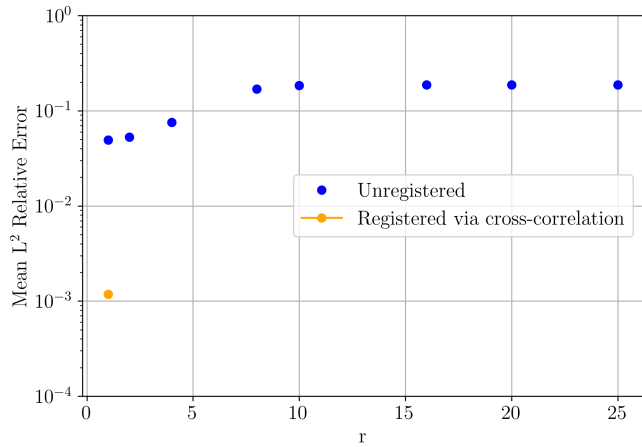


Figure 12: Comparison of mean relative L_2 prediction error for 2D isentropic convective vortex test set parameters using POD-RBF-ROM, presented for the unregistered case (without registration) and the registered case (with registration via cross-correlation).

In Figure 12, we illustrate the mean relative L_2 prediction error for test set param-

eters across different POD ranks in the construction of POD-RBF-ROM, using both unregistered and registered snapshots via cross-correlation. The results show that in the unregistered case, even with 25 modes, the ROM remains inefficient and inaccurate, yielding errors that are two orders of magnitude higher than in the registered case. Conversely, in the registered case, the first POD mode retaining 99.99 % of the cumulative energy is sufficient to yield efficient and accurate ROM.

6 Conclusion

In this work, we employ cross-correlation based snapshot registration for model reduction of transport-dominated problems. This cross-correlation based registration accelerates the KnW decay, facilitating the construction of a low-dimensional linear approximation subspace for efficient ROM development. We propose a complete framework comprising offline-online stages for the construction of ROMs using the cross-correlation based snapshots registration. We tested our proposed workflow on transport-dominated problems: 1D travelling waves, and 2D isentropic vortex. In both numerical experiments, the proposed approach results in efficient and accurate ROMs. However, the applicability of this approach is confined to certain transport-dominated problems where the structures of the transported features remain consistent. This approach is not suitable for addressing advection-diffusion problems.

Snapshot registration has seen significant advancements in medical imaging, largely driven by the progress of deep learning frameworks. Methods such as VoxelMorph [1], LapIRN [29], and FAIM (FAST Image Registration) [25] have demonstrated both speed and accuracy. These methods can be integrated within model reduction frameworks to address the challenges posed by slow KnW decay.

Acknowledgements

We acknowledge the PhD grant supported by industrial partner Danieli & C. S.p.A. and Programma Operativo Nazionale Ricerca e Innovazione 2014-2020, P.I. Gianluigi Rozza. GS acknowledges the financial support under the National Recovery and Resilience Plan (NRRP), Mission 4, Component 2, Investment 1.1, Call for tender No. 1409 published on 14.9.2022 by the Italian Ministry of University and Research (MUR), funded by the European Union – NextGenerationEU– Project Title ROMEU – CUP P2022FEZS3 - Grant Assignment Decree No. 1379 adopted on 01/09/2023 by the Italian Ministry of Ministry of University and Research (MUR) and acknowledges the financial support by the European Union (ERC, DANTE, GA-101115741). Views and opinions expressed are however, those of the author(s) only and do not necessarily reflect those of the European Union or the European Research Council Executive Agency. Neither the European Union nor the granting authority can be held responsible for them.

CRediT authorship contribution statement

Harshith Gowrachari: Writing - original draft, Conceptualization, Data curation, Formal Analysis, Visualization, Methodology, Software. Giovanni Stabile: Writing – review & editing, Supervision. Gianluigi Rozza: Writing – review & editing, Funding acquisition, Project administration, Supervision.

Data Statement

The results presented can be reproduced by following the public repository at <https://github.com/harshith-gowrachari/MOR-CrossCorr-Registration>, which contains Jupyter notebooks for these numerical experiments. In this framework, we use the `scipy` library to compute cross-correlation and `EZyRB` package (<https://github.com/mathLab/EZyRB>) [10], an open-source `Python` library for non-intrusive data-driven model order reduction of parameterized problems, developed and maintained at SISSA mathLab.

References

- [1] G. Balakrishnan, A. Zhao, M. R. Sabuncu, J. Guttag, and A. V. Dalca. Voxelmorph: A learning framework for deformable medical image registration. *IEEE Transactions on Medical Imaging*, 38(8):1788–1800, Aug. 2019. ISSN 1558-254X. doi: 10.1109/tmi.2019.2897538. URL <http://dx.doi.org/10.1109/TMI.2019.2897538>.
- [2] J. Barnett and C. Farhat. Quadratic approximation manifold for mitigating the Kolmogorov barrier in nonlinear projection-based model order reduction. *Journal of Computational Physics*, 464:111348, Sept. 2022. ISSN 0021-9991. doi: 10.1016/j.jcp.2022.111348. URL <http://dx.doi.org/10.1016/j.jcp.2022.111348>.
- [3] K. Berberidis and I. Karybali. A new efficient cross-correlation based image registration technique with improved performance. In *2002 11th European Signal Processing Conference*, pages 1–4. IEEE, 2002.
- [4] J. Bruna, B. Peherstorfer, and E. Vanden-Eijnden. Neural Galerkin schemes with active learning for high-dimensional evolution equations. *Journal of Computational Physics*, 496:112588, Jan. 2024. ISSN 0021-9991. doi: 10.1016/j.jcp.2023.112588. URL <http://dx.doi.org/10.1016/j.jcp.2023.112588>.
- [5] N. Cagniart, R. Crisovan, Y. Maday, and R. Abgrall. Model Order Reduction for Hyperbolic Problems: a new framework. *HAL archive*, 2017. URL <https://hal.science/hal-01583224>.
- [6] S. Chelbi and A. Mekhmoukh. Features based image registration using cross correlation and radon transform. *Alexandria engineering journal*, 57(4):2313–2318, 2018.

- [7] F. Chinesta, A. Huerta, G. Rozza, and K. Willcox. Model reduction methods. *Encyclopedia of Computational Mechanics Second Edition*, page 1–36, Dec. 2017. doi: 10.1002/9781119176817.ecm2110. URL <http://dx.doi.org/10.1002/9781119176817.ecm2110>.
- [8] R. Crisovan, D. Torlo, R. Abgrall, and S. Tokareva. Model order reduction for parametrized nonlinear hyperbolic problems as an application to uncertainty quantification. *Journal of Computational and Applied Mathematics*, 348:466–489, March 2019. ISSN 0377-0427. doi: 10.1016/j.cam.2018.09.018. URL <http://dx.doi.org/10.1016/j.cam.2018.09.018>.
- [9] G. Debojyoti, L. John, and Y. Kim. HyPar 1.0 - Finite-Difference Hyperbolic-Parabolic PDE Solver on Cartesian Grids. <https://github.com/debog/hypar>, n.d. URL <https://hypar.github.io/index.html>.
- [10] N. Demo, M. Tezzele, and G. Rozza. EZyRB: Easy Reduced Basis method. ”<https://github.com/mathLab/EZyRB>”, April 2018. ISSN 2475-9066. URL <http://dx.doi.org/10.21105/joss.00661>.
- [11] C. Eckart and G. Young. The approximation of one matrix by another of lower rank. *Psychometrika*, 1(3):211–218, Sept. 1936. ISSN 1860-0980. doi: 10.1007/bf02288367. URL <http://dx.doi.org/10.1007/BF02288367>.
- [12] S. Fresca, L. Dede’, and A. Manzoni. A Comprehensive Deep Learning-Based Approach to Reduced Order Modeling of Nonlinear Time-Dependent Parametrized PDEs. *Journal of Scientific Computing*, 87(2), April 2021. ISSN 1573-7691. doi: 10.1007/s10915-021-01462-7. URL <http://dx.doi.org/10.1007/s10915-021-01462-7>.
- [13] R. Geelen, S. Wright, and K. Willcox. Operator inference for non-intrusive model reduction with quadratic manifolds. *Computer Methods in Applied Mechanics and Engineering*, 403:115717, Jan. 2023. ISSN 0045-7825. doi: 10.1016/j.cma.2022.115717. URL <http://dx.doi.org/10.1016/j.cma.2022.115717>.
- [14] S. Gottlieb, C.-W. Shu, and E. Tadmor. Strong Stability-Preserving High-Order Time Discretization Methods. *SIAM Review*, 43(1):89–112, Jan. 2001. ISSN 1095-7200. doi: 10.1137/s003614450036757x. URL <http://dx.doi.org/10.1137/S003614450036757X>.
- [15] H. Gowrachari, N. Demo, G. Stabile, and G. Rozza. Non-intrusive model reduction of advection-dominated hyperbolic problems using neural network shift augmented manifold transformations, 2024. URL <https://arxiv.org/abs/2407.18419>.
- [16] B. Haasdonk and M. Ohlberger. Adaptive basis enrichment for the reduced basis method applied to finite volume schemes. In *Proceedings of the 5th International Symposium on Finite Volumes for Complex Applications*, pages 471–478, 2008.

- [17] D. Hartman and L. K. Mestha. A deep learning framework for model reduction of dynamical systems. In *2017 IEEE Conference on Control Technology and Applications (CCTA)*. IEEE, Aug. 2017. doi: 10.1109/ccta.2017.8062736. URL <http://dx.doi.org/10.1109/CCTA.2017.8062736>.
- [18] J. S. Hesthaven, G. Rozza, and B. Stamm. *Certified Reduced Basis Methods for Parametrized Partial Differential Equations*. Springer International Publishing, 2016. ISBN 9783319224701. doi: 10.1007/978-3-319-22470-1. URL <http://dx.doi.org/10.1007/978-3-319-22470-1>.
- [19] C. Hoang, K. Chowdhary, K. Lee, and J. Ray. Projection-based model reduction of dynamical systems using space–time subspace and machine learning. *Computer Methods in Applied Mechanics and Engineering*, 389:114341, Feb. 2022. ISSN 0045-7825. doi: 10.1016/j.cma.2021.114341. URL <http://dx.doi.org/10.1016/j.cma.2021.114341>.
- [20] A. Iollo and D. Lombardi. Advection modes by optimal mass transfer. *Physical Review E*, 89(2), Feb. 2014. ISSN 1550-2376. doi: 10.1103/physreve.89.022923. URL <http://dx.doi.org/10.1103/PhysRevE.89.022923>.
- [21] O. Issan and B. Kramer. Predicting solar wind streams from the inner-heliosphere to earth via shifted operator inference. *Journal of Computational Physics*, 473: 111689, Jan. 2023. ISSN 0021-9991. doi: 10.1016/j.jcp.2022.111689. URL <http://dx.doi.org/10.1016/j.jcp.2022.111689>.
- [22] S. Jain, P. Tiso, J. B. Rutzmoser, and D. J. Rixen. A quadratic manifold for model order reduction of nonlinear structural dynamics. *Computers & Structures*, 188: 80–94, Aug. 2017. ISSN 0045-7949. doi: 10.1016/j.compstruc.2017.04.005. URL <http://dx.doi.org/10.1016/j.compstruc.2017.04.005>.
- [23] K. Kashima. Nonlinear model reduction by deep autoencoder of noise response data. In *2016 IEEE 55th Conference on Decision and Control (CDC)*. IEEE, Dec. 2016. doi: 10.1109/cdc.2016.7799153. URL <http://dx.doi.org/10.1109/CDC.2016.7799153>.
- [24] Y. Kim, Y. Choi, D. Widemann, and T. Zohdi. A fast and accurate physics-informed neural network reduced order model with shallow masked autoencoder. *Journal of Computational Physics*, 451:110841, Feb. 2022. ISSN 0021-9991. doi: 10.1016/j.jcp.2021.110841. URL <http://dx.doi.org/10.1016/j.jcp.2021.110841>.
- [25] D. Kuang and T. Schmah. *FAIM – A ConvNet Method for Unsupervised 3D Medical Image Registration*, page 646–654. Springer International Publishing, 2019. ISBN 9783030326920. doi: 10.1007/978-3-030-32692-0_74. URL http://dx.doi.org/10.1007/978-3-030-32692-0_74.
- [26] K. Lee and K. T. Carlberg. Model reduction of dynamical systems on nonlinear manifolds using deep convolutional autoencoders. *Journal of Computational*

Physics, 404:108973, March 2020. ISSN 0021-9991. doi: 10.1016/j.jcp.2019.108973. URL <http://dx.doi.org/10.1016/j.jcp.2019.108973>.

- [27] R. Mojgani and M. Balajewicz. Lagrangian basis method for dimensionality reduction of convection dominated nonlinear flows. *ArXiv*, abs/1701.04343, 2017. URL <https://api.semanticscholar.org/CorpusID:119505364>.
- [28] R. Mojgani and M. Balajewicz. Arbitrary Lagrangian Eulerian framework for efficient projection-based reduction of convection dominated nonlinear flows. In *APS Division of Fluid Dynamics Meeting Abstracts*, pages M1–008, 2017.
- [29] T. C. W. Mok and A. C. S. Chung. *Large Deformation Diffeomorphic Image Registration with Laplacian Pyramid Networks*, page 211–221. Springer International Publishing, 2020. ISBN 9783030597160. doi: 10.1007/978-3-030-59716-0_21. URL http://dx.doi.org/10.1007/978-3-030-59716-0_21.
- [30] M. Nonino and D. Torlo. Calibration-based ale model order reduction for hyperbolic problems with self-similar travelling discontinuities. *Journal of Scientific Computing*, 101(3), Oct. 2024. ISSN 1573-7691. doi: 10.1007/s10915-024-02694-z. URL <http://dx.doi.org/10.1007/s10915-024-02694-z>.
- [31] M. Nonino, F. Ballarin, G. Rozza, and Y. Maday. A reduced basis method by means of transport maps for a fluid–structure interaction problem with slowly decaying kolmogorov n -width. *Advances in Computational Science and Engineering*, 1(1): 36–58, 2023. ISSN 2837-1739. doi: 10.3934/acse.2023002. URL <http://dx.doi.org/10.3934/acse.2023002>.
- [32] M. Ohlberger and S. Rave. Nonlinear reduced basis approximation of parameterized evolution equations via the method of freezing. *Comptes Rendus. Mathématique*, 351(23–24):901–906, Nov. 2013. ISSN 1778-3569. doi: 10.1016/j.crma.2013.10.028. URL <http://dx.doi.org/10.1016/j.crma.2013.10.028>.
- [33] B. Peherstorfer. Model Reduction for Transport-Dominated Problems via Online Adaptive Bases and Adaptive Sampling. *SIAM Journal on Scientific Computing*, 42(5):A2803–A2836, Jan. 2020. ISSN 1095-7197. doi: 10.1137/19m1257275. URL <http://dx.doi.org/10.1137/19M1257275>.
- [34] B. Peherstorfer. Breaking the Kolmogorov Barrier with Nonlinear Model Reduction. *Notices of the American Mathematical Society*, 69(05):1, May 2022. ISSN 1088-9477. doi: 10.1090/noti2475. URL <http://dx.doi.org/10.1090/noti2475>.
- [35] B. Peherstorfer and K. Willcox. Online Adaptive Model Reduction for Nonlinear Systems via Low-Rank Updates. *SIAM Journal on Scientific Computing*, 37(4): A2123–A2150, Jan. 2015. ISSN 1095-7197. doi: 10.1137/140989169. URL <http://dx.doi.org/10.1137/140989169>.

- [36] B. Peherstorfer and K. Willcox. Data-driven operator inference for nonintrusive projection-based model reduction. *Computer Methods in Applied Mechanics and Engineering*, 306:196–215, July 2016. ISSN 0045-7825. doi: 10.1016/j.cma.2016.03.025. URL <http://dx.doi.org/10.1016/j.cma.2016.03.025>.
- [37] A. Pinkus. *n-Widths in Approximation Theory*. Springer Berlin Heidelberg, 1985. ISBN 9783642698941. doi: 10.1007/978-3-642-69894-1. URL <http://dx.doi.org/10.1007/978-3-642-69894-1>.
- [38] A. Quarteroni, A. Manzoni, and F. Negri. *Reduced Basis Methods for Partial Differential Equations*. Springer International Publishing, 2016. ISBN 9783319154312. doi: 10.1007/978-3-319-15431-2. URL <http://dx.doi.org/10.1007/978-3-319-15431-2>.
- [39] D. Rim, S. Moe, and R. J. LeVeque. Transport Reversal for Model Reduction of Hyperbolic Partial Differential Equations. *SIAM/ASA Journal on Uncertainty Quantification*, 6(1):118–150, Jan. 2018. ISSN 2166-2525. doi: 10.1137/17m1113679. URL <http://dx.doi.org/10.1137/17M1113679>.
- [40] F. Romor, G. Stabile, and G. Rozza. Non-linear Manifold Reduced-Order Models with Convolutional Autoencoders and Reduced Over-Collocation Method. *Journal of Scientific Computing*, 94(3), Feb. 2023. ISSN 1573-7691. doi: 10.1007/s10915-023-02128-2. URL <http://dx.doi.org/10.1007/s10915-023-02128-2>.
- [41] G. Rozza, G. Stabile, and F. Ballarin. *Advanced Reduced Order Methods and Applications in Computational Fluid Dynamics*. Society for Industrial and Applied Mathematics, Jan 2022. ISBN 9781611977257. doi: 10.1137/1.9781611977257. URL <http://dx.doi.org/10.1137/1.9781611977257>.
- [42] C.-W. Shu. *Essentially non-oscillatory and weighted essentially non-oscillatory schemes for hyperbolic conservation laws*, page 325–432. Springer Berlin Heidelberg, 1998. ISBN 9783540498049. doi: 10.1007/bfb0096355. URL <http://dx.doi.org/10.1007/BFb0096355>.
- [43] S. C. Spiegel, H. Huynh, and J. R. DeBonis. A survey of the isentropic euler vortex problem using high-order methods. In *22nd AIAA Computational Fluid Dynamics Conference*. American Institute of Aeronautics and Astronautics, June 2015. doi: 10.2514/6.2015-2444. URL <http://dx.doi.org/10.2514/6.2015-2444>.
- [44] G. Stabile and G. Rozza. Finite volume pod-galerkin stabilised reduced order methods for the parametrised incompressible navier–stokes equations. *Computers & Fluids*, 173:273–284, Sept. 2018. ISSN 0045-7930. doi: 10.1016/j.compfluid.2018.01.035. URL <http://dx.doi.org/10.1016/j.compfluid.2018.01.035>.
- [45] G. Stabile, F. Ballarin, G. Zuccarino, and G. Rozza. A reduced order variational multiscale approach for turbulent flows. *Advances in Computational Mathematics*,

45(5–6):2349–2368, June 2019. ISSN 1572-9044. doi: 10.1007/s10444-019-09712-x. URL <http://dx.doi.org/10.1007/s10444-019-09712-x>.

[46] G. W. Stewart. On the Early History of the Singular Value Decomposition. *SIAM Review*, 35(4):551–566, Dec 1993. ISSN 1095-7200. doi: 10.1137/1035134. URL <http://dx.doi.org/10.1137/1035134>.

[47] T. Taddei. A Registration Method for Model Order Reduction: Data Compression and Geometry Reduction. *SIAM Journal on Scientific Computing*, 42(2):A997–A1027, Jan. 2020. ISSN 1095-7197. doi: 10.1137/19m1271270. URL <http://dx.doi.org/10.1137/19M1271270>.

[48] M. Tezzele, N. Demo, G. Stabile, and G. Rozza. *Chapter 9: Nonintrusive Data-Driven Reduced Order Models in Computational Fluid Dynamics*, page 203–222. Society for Industrial and Applied Mathematics, Jan. 2022. ISBN 9781611977257. doi: 10.1137/1.9781611977257.ch9. URL <http://dx.doi.org/10.1137/1.9781611977257.ch9>.

[49] D. Torlo. Model Reduction for Advection Dominated Hyperbolic Problems in an ALE Framework: Offline and Online Phases. *arXiv preprint*, March 2020. doi: 10.48550/arxiv.2003.13735. URL <https://arxiv.org/abs/2003.13735>.

[50] Z. Wang, K. Fidkowski, R. Abgrall, F. Bassi, D. Caraeni, A. Cary, H. Deconinck, R. Hartmann, K. Hillewaert, H. Huynh, N. Kroll, G. May, P. Persson, B. van Leer, and M. Visbal. High-order cfd methods: current status and perspective. *International Journal for Numerical Methods in Fluids*, 72(8):811–845, Jan. 2013. ISSN 1097-0363. doi: 10.1002/fld.3767. URL <http://dx.doi.org/10.1002/fld.3767>.

[51] K. Washabaugh, D. Amsallem, M. Zahr, and C. Farhat. Nonlinear Model Reduction for CFD Problems Using Local Reduced-Order Bases. In *42nd AIAA Fluid Dynamics Conference and Exhibit*. American Institute of Aeronautics and Astronautics, June 2012. doi: 10.2514/6.2012-2686. URL <http://dx.doi.org/10.2514/6.2012-2686>.

[52] Y.-T. Zhang and C.-W. Shu. ENO and WENO Schemes . In *Handbook of Numerical Methods for Hyperbolic Problems - Basic and Fundamental Issues*, page 103–122. Elsevier, 2016. doi: 10.1016/bs.hna.2016.09.009. URL <http://dx.doi.org/10.1016/bs.hna.2016.09.009>.